3D Tomography of Magnetic Field by Opt. Polarimetry and Gaia Distances

Y. Doi (U. Tokyo), K.Kawabata, K.Nakamura,
T.Hori (Hiroshima U.), M.Matsumura (Kagawa U.),
H.Akitaya (Chiba Inst. Tech.), et al.

Magnetic field position angle decomposition per distance

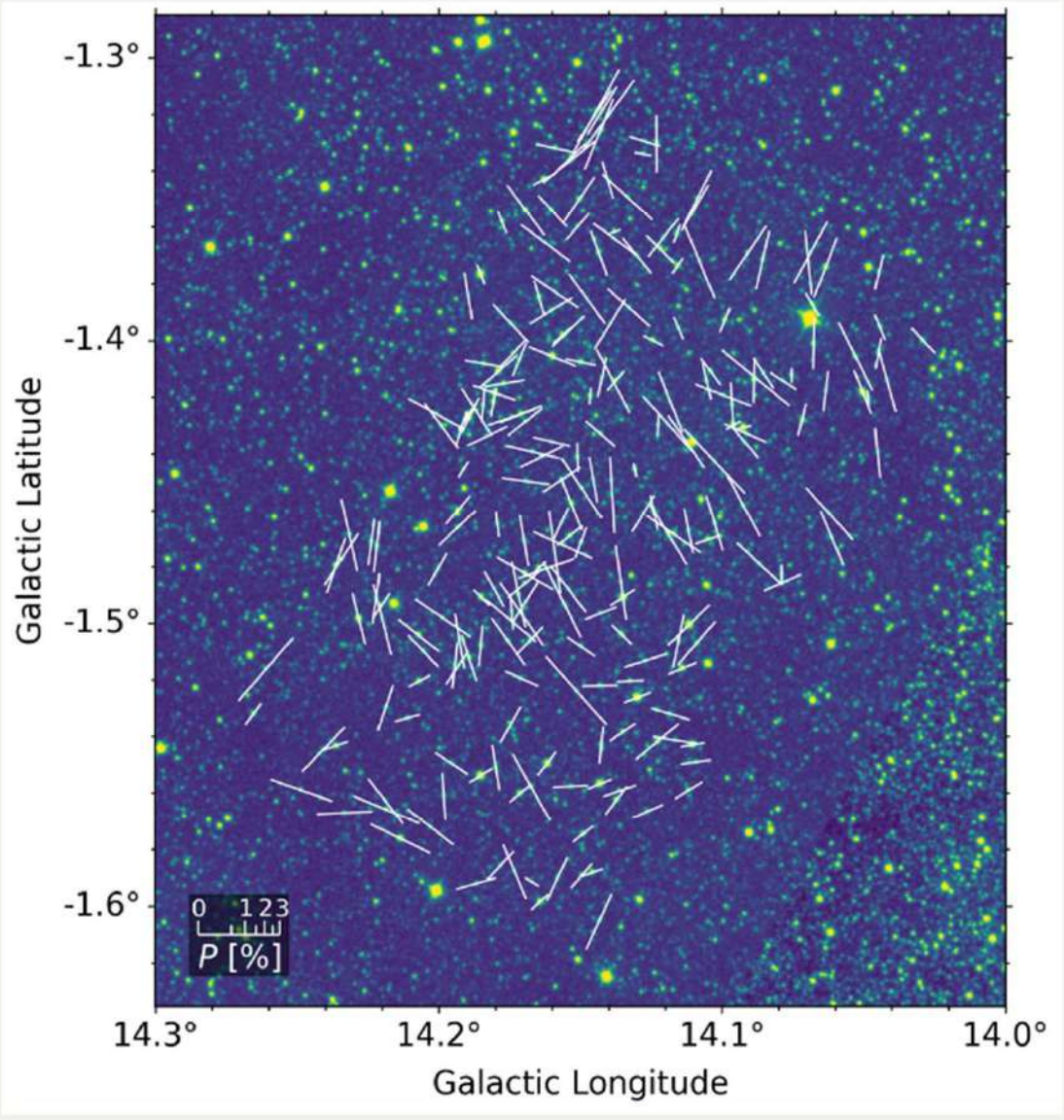

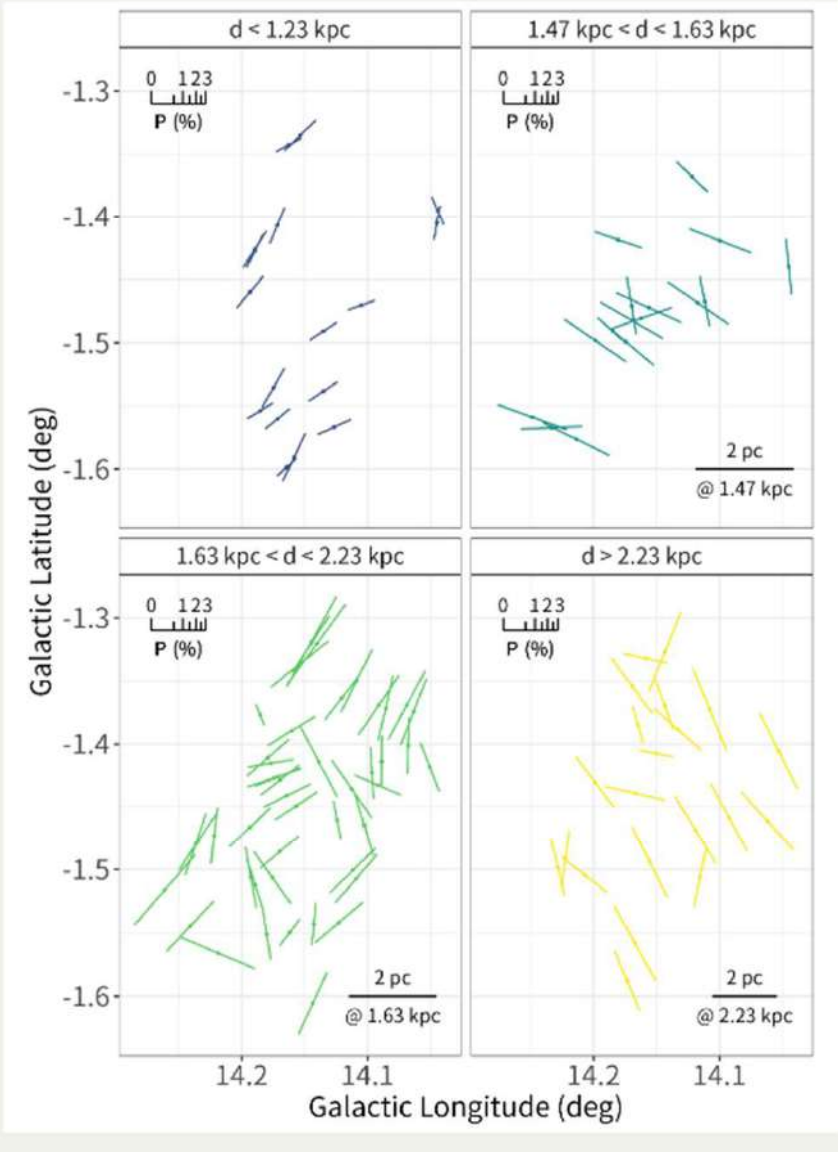

3D *B*-field structure (Perseus)

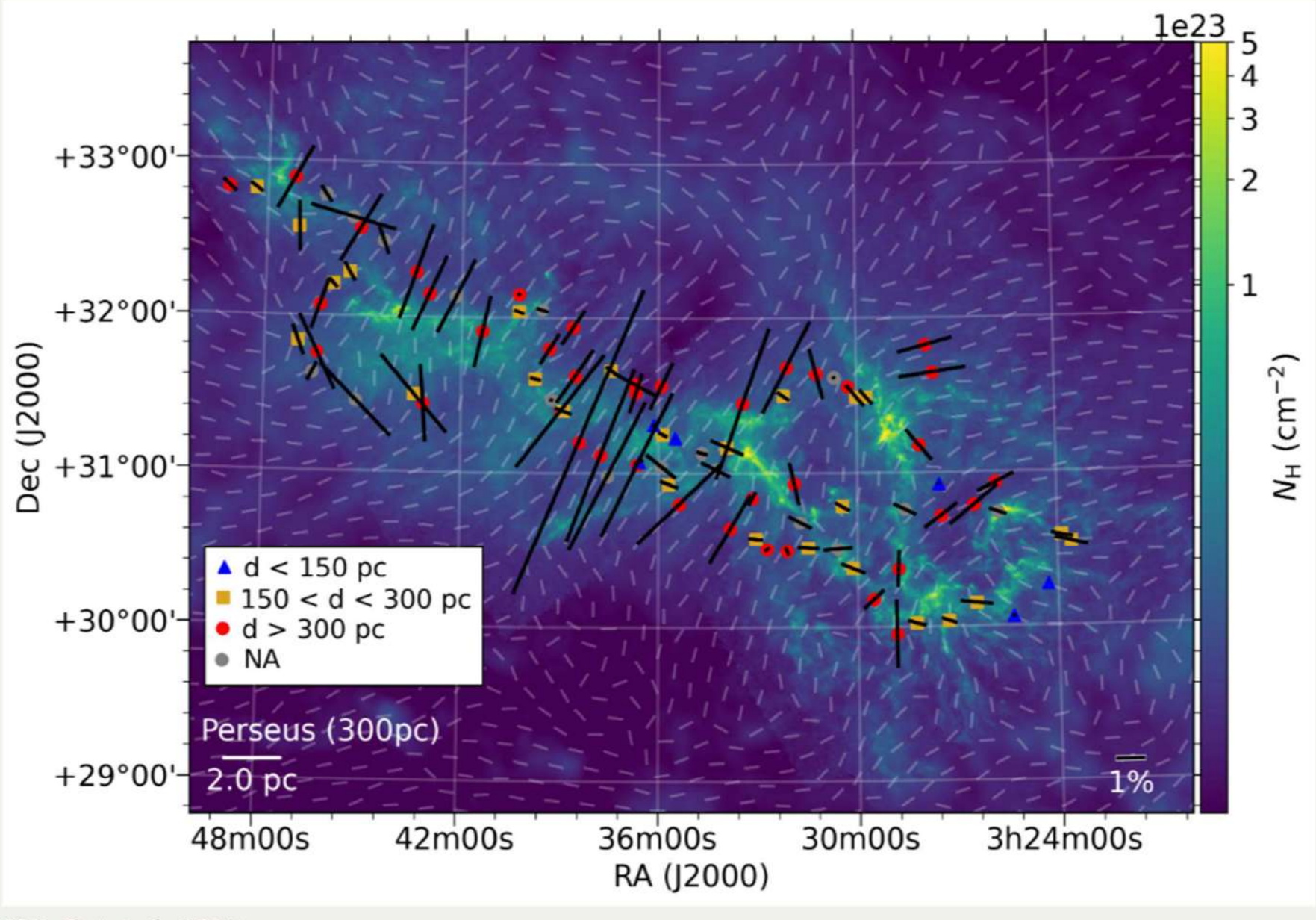

Goodman et al. (1990), Doi et al. (2021)

Stellar distances (obs. by *Gaia*)

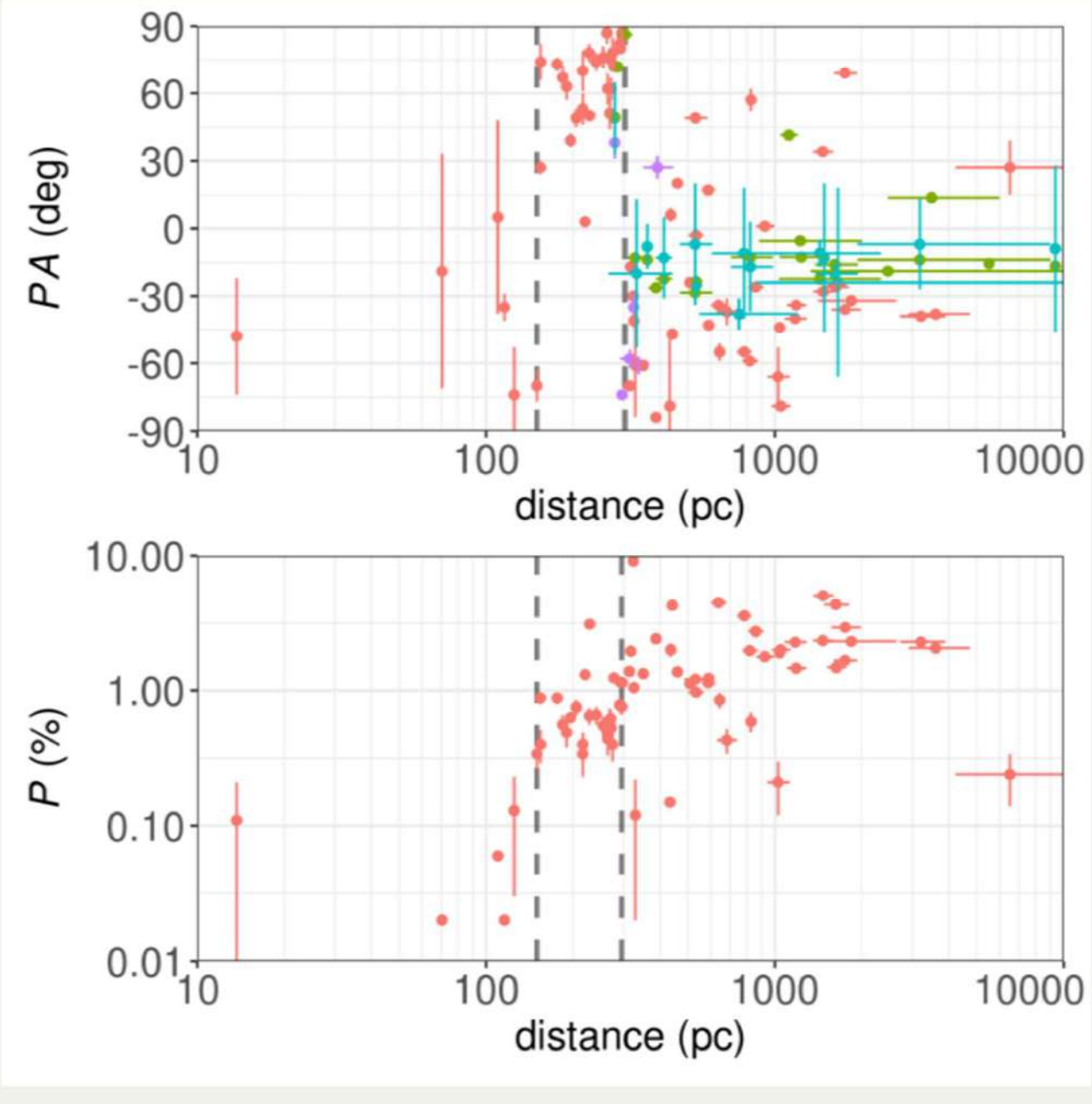

breakpoints

- *PA*
  - 150^{+4}_{-34} (pc)
  - 303^{+12}_{-7} (pc)
- *P*
  - 150^{+4}_{-136} (pc)
  - 295^{+22}_{-67} (pc)

Opt. (Goodman+1990)
R (Alves+2011)
J (Alves+2011)
K (Tamura+1988)

The Breakspoint Analysis

1. assume a stepwise change of a parameter as a function of distance
2. estimate positions of abrupt change (= breakpoints) as a maximum likelihood estimation
    - number of breakpoints is assumed in this analysis
3. change the number of breakpoints and repeat the evaluation, estimate BIC as a goodness of fit
4. find the number of breakpoints that gives the minimum value of BIC

Both the polarization position angle and polarization fraction give two breakpoints consistently.

Two layers of vertically distinct *B*-fields for Perseus (300 pc) and Taurus (150 pc)

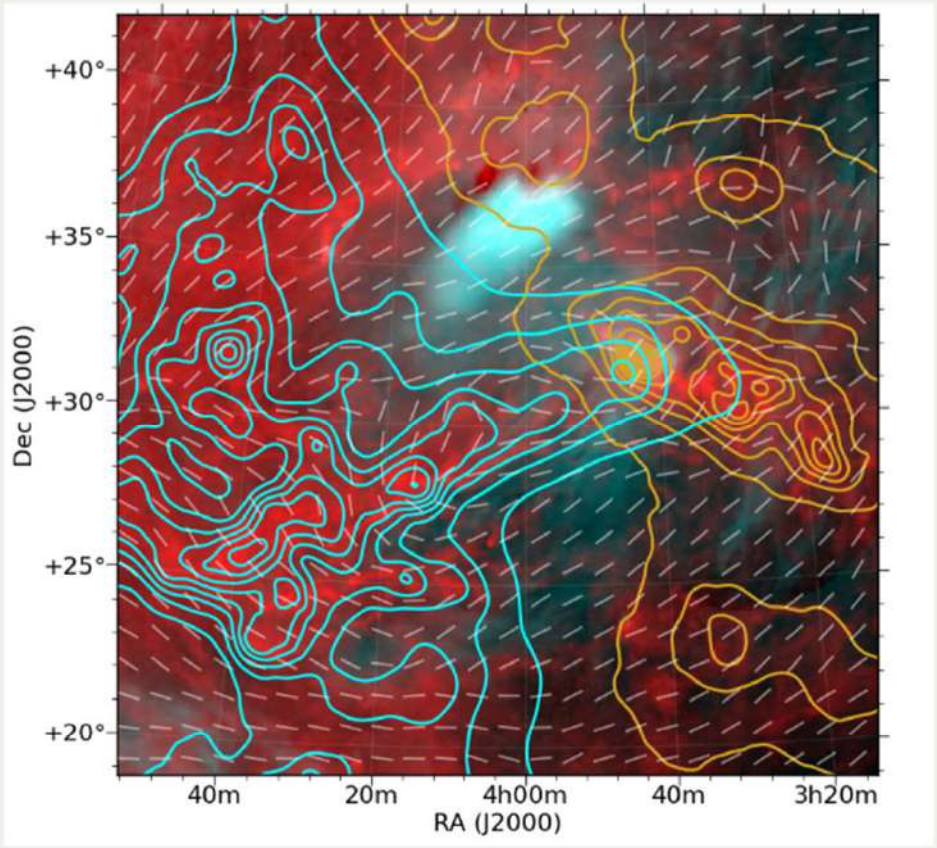

Contours: dust column density based on *Gaia* extinction (Leike et al. 2018)

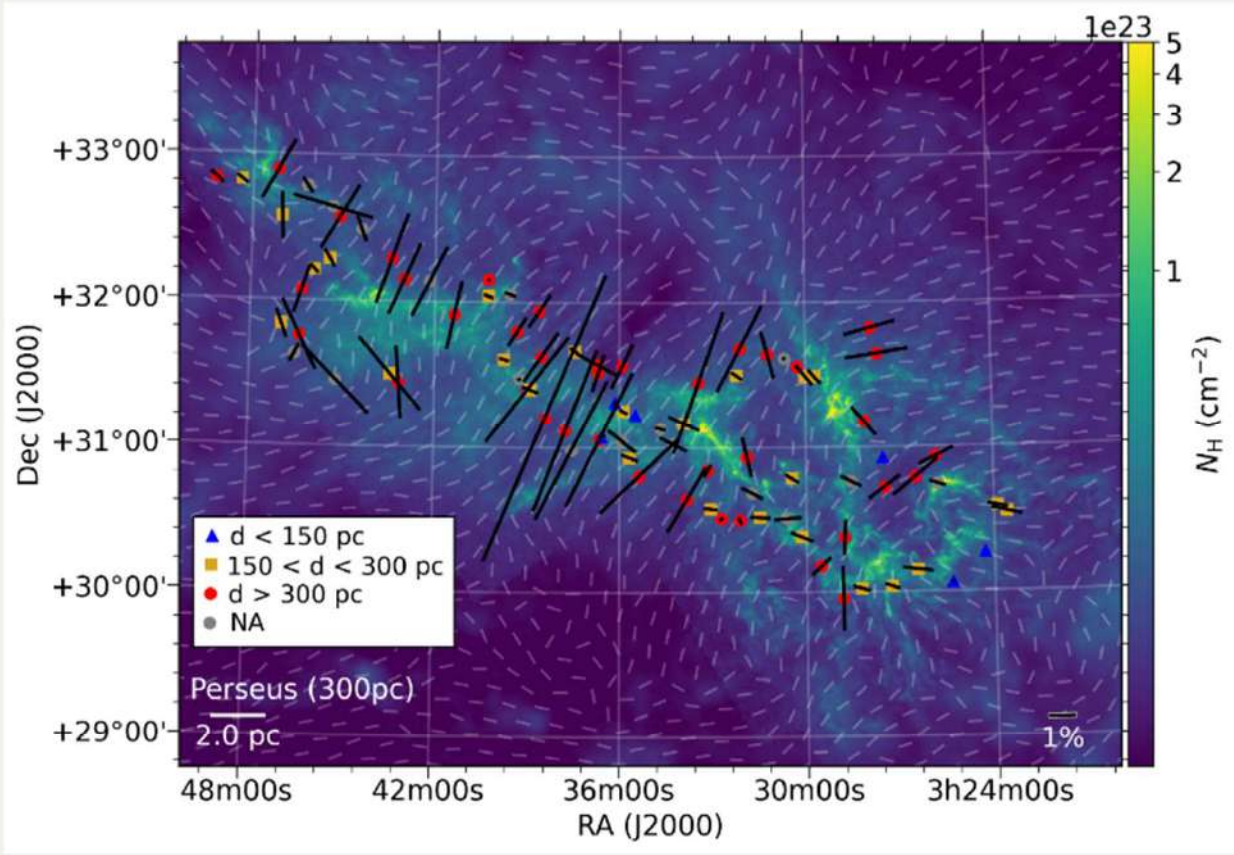

Doi et al. (2021)

B-field at the frontside and the backside of the dust "cavity"

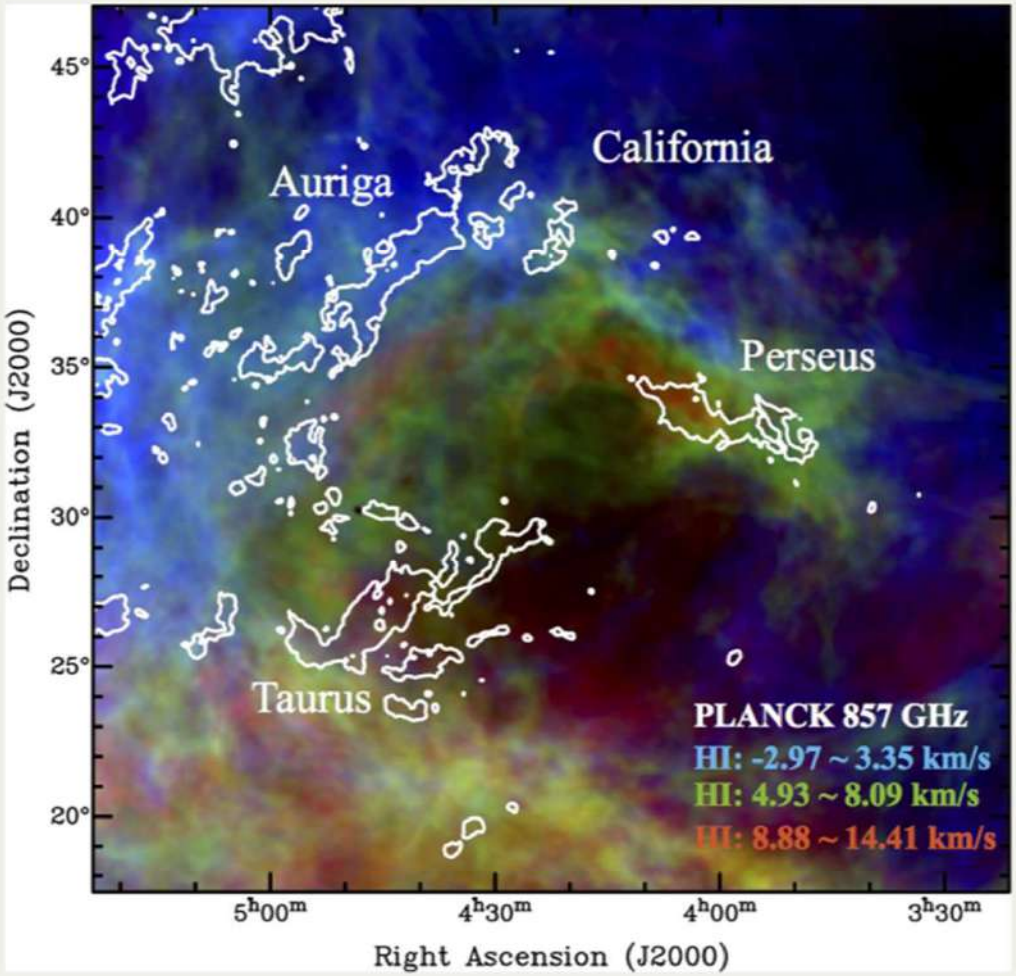

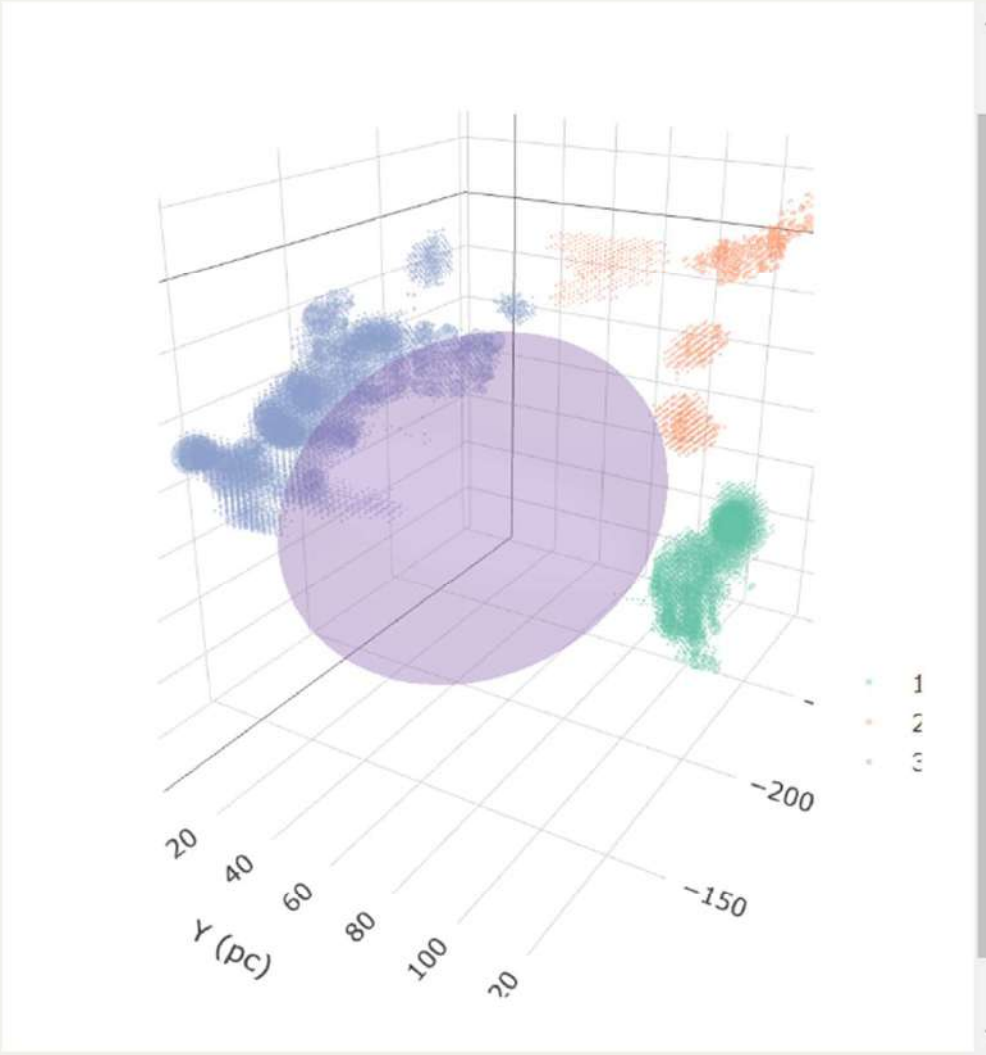

Per OB2 bubble by Shimajiri et al. (2019)

Polarimetric survey programs

- RoboPol $\leftarrow b \geqslant 30^\circ$
- SOUTH POL $\leftarrow b \leqslant -30^\circ$
  - Both targeting CMB foreground separation
- GPIPS $\leftarrow l = +18^\circ \sim +56^\circ,\ b = -1^\circ \sim +1^\circ$
  - Heavy obscuration by the local clouds
- SGMAP $\leftarrow$ a polarimetric survey project led by **Hiroshima Univ. (広島大)**

HONIR on KANATA 1.5-m telescope, Hiroshima

- HONIR: Hiroshima Optical and Near-InfraRed camera

KANATA telescope, HIROSHIMA

Hiroshima Optical and Near-infrared Camera

HONIR: Hiroshima Optical and Near-InfraRed camera

HONIR is an instrument for the 1.5-m Kanata telescope at Higashi-Hiroshima Observatory, Hiroshima Astrophysical Science Center, Hiroshima University.

HONIR is capable of obtaining two color (optical (0.5-1.0 μm) and near-infrared (1.0-2.0μm)) images or spectra simultaneously with an optional linear imaging polarimetry and spectro-polarimetry functions. The field of view of the imaging mode is 10 arcmin square with a spatial sampling of 0".29.

Targeting the Sagittarius arm

- Narrow FoV $\leftrightarrow$ longer depth along LoS
- Moderate A_{V}, moderately complicated B_{POS}
  - Referring to Gaia A_{G}, Optical/Planck B_{POS}

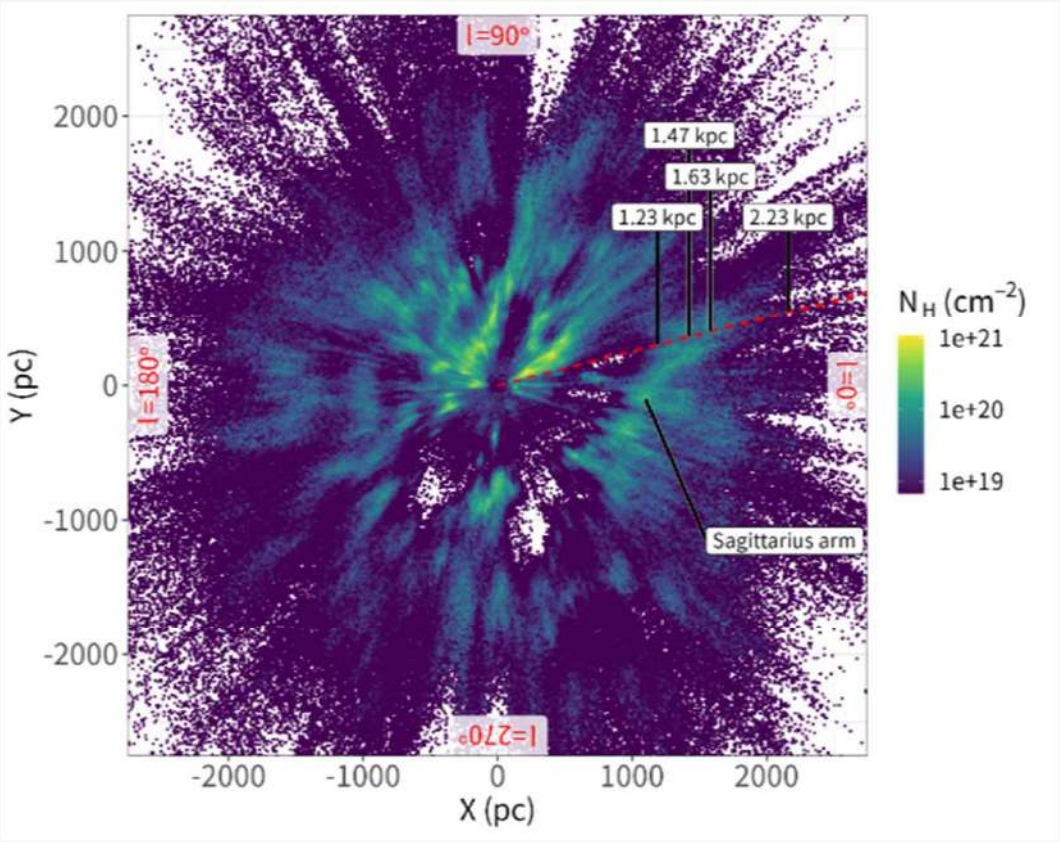

Doi et al. (in prep)

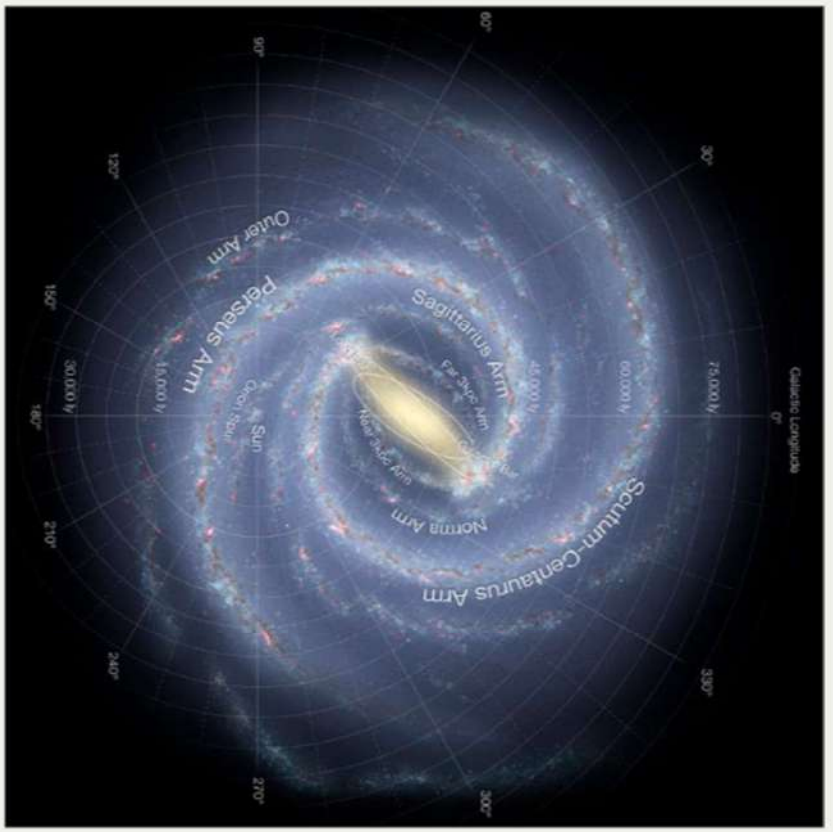

Credit: NASA/JPL-Caltech/ESO/R. Hurt

Galactic magnetic field

- Magnetic field model: normally consists of `disc' + `halo' (+ `GC')

NASA press release (2021)

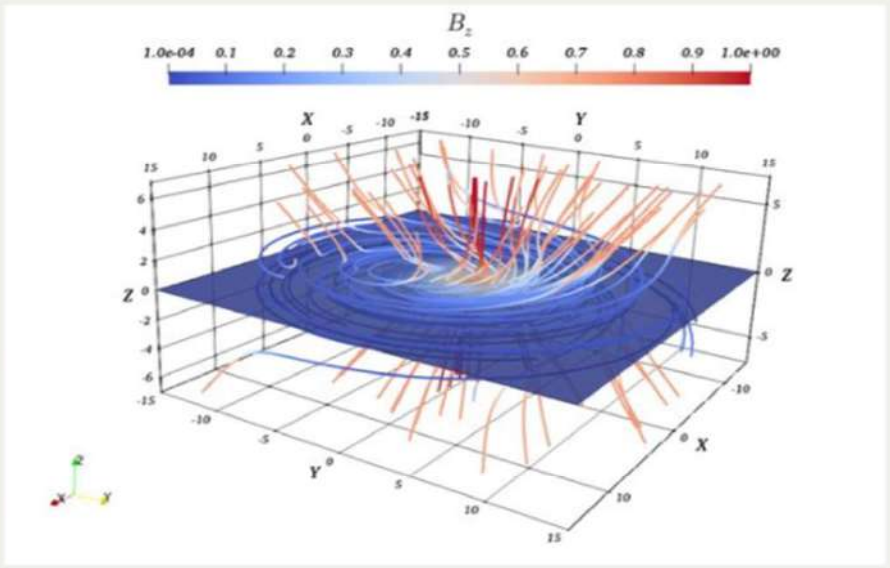

Cerri et al. (2017)

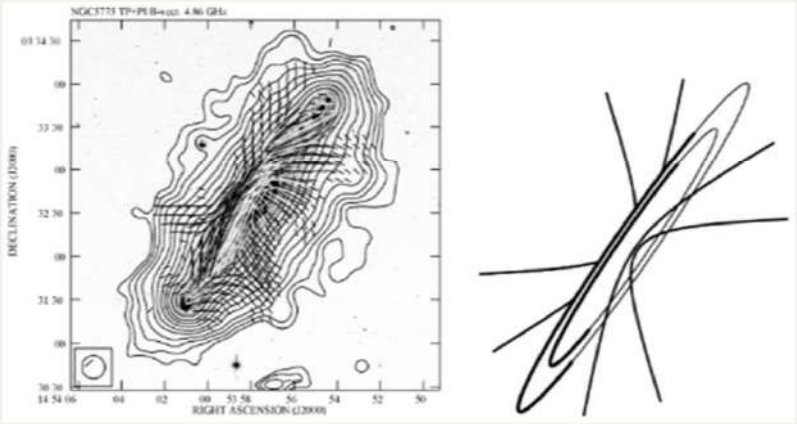

Soida et al. (2011)

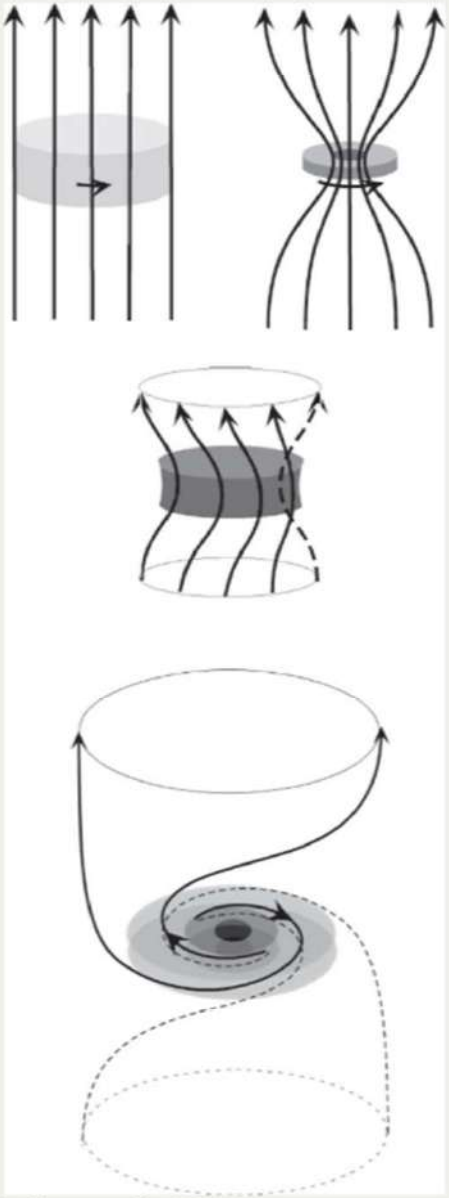

Sofue et al. (2010)

B-field morphology in the arms

- Disc components: parallel to disc, stretching along galactic arms (both Galactic & extragalactic *B*-field)
- Global/small-scale random component: distribution is unkown
- Off-plane galactic disc component: not well observed

NASA (2021)

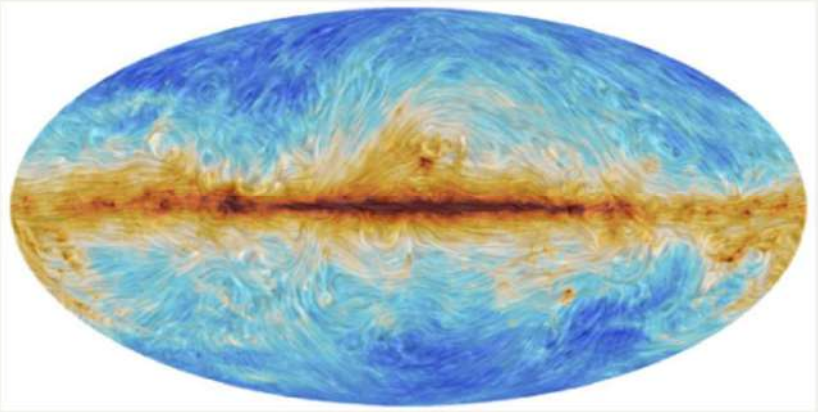

Planck Collaboration et al. (2016)

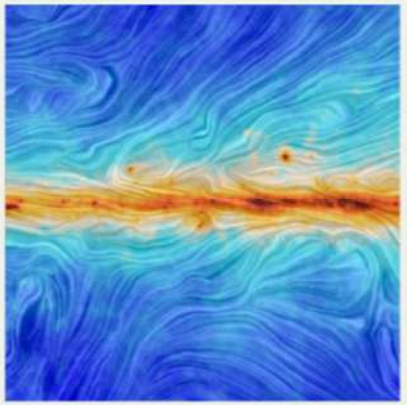

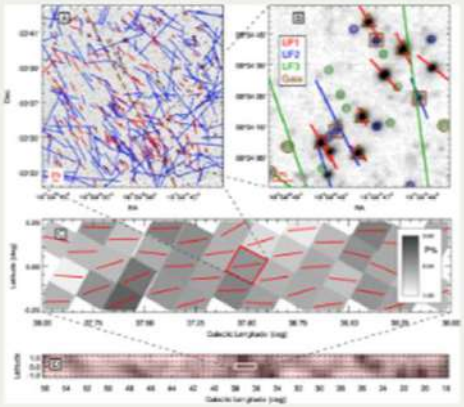

Clemens et al.(2020)

Previous researches

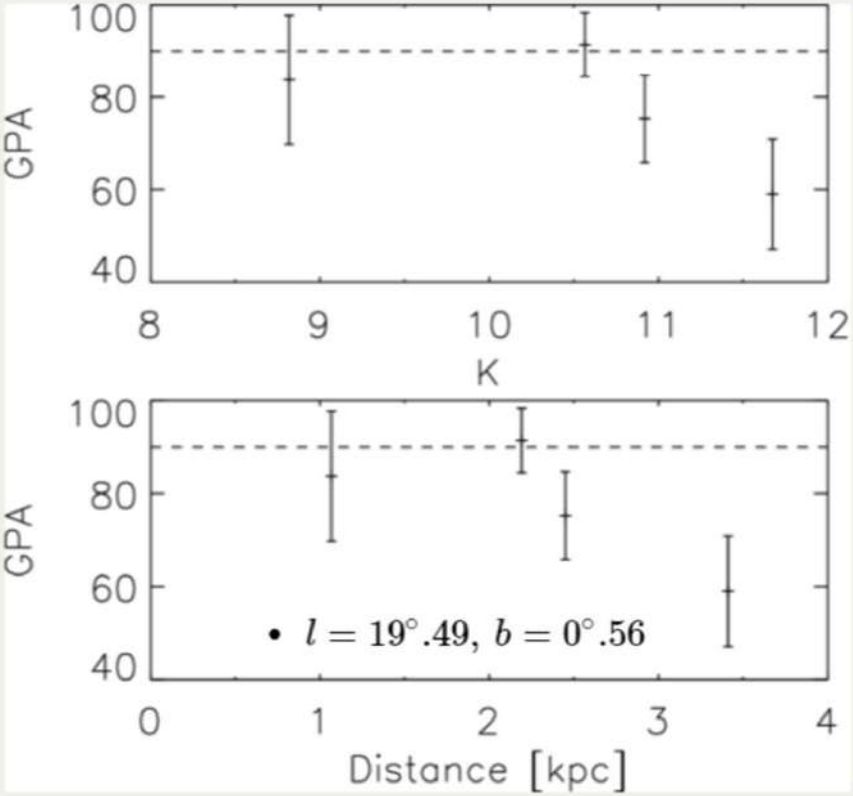

Pavel (2014)

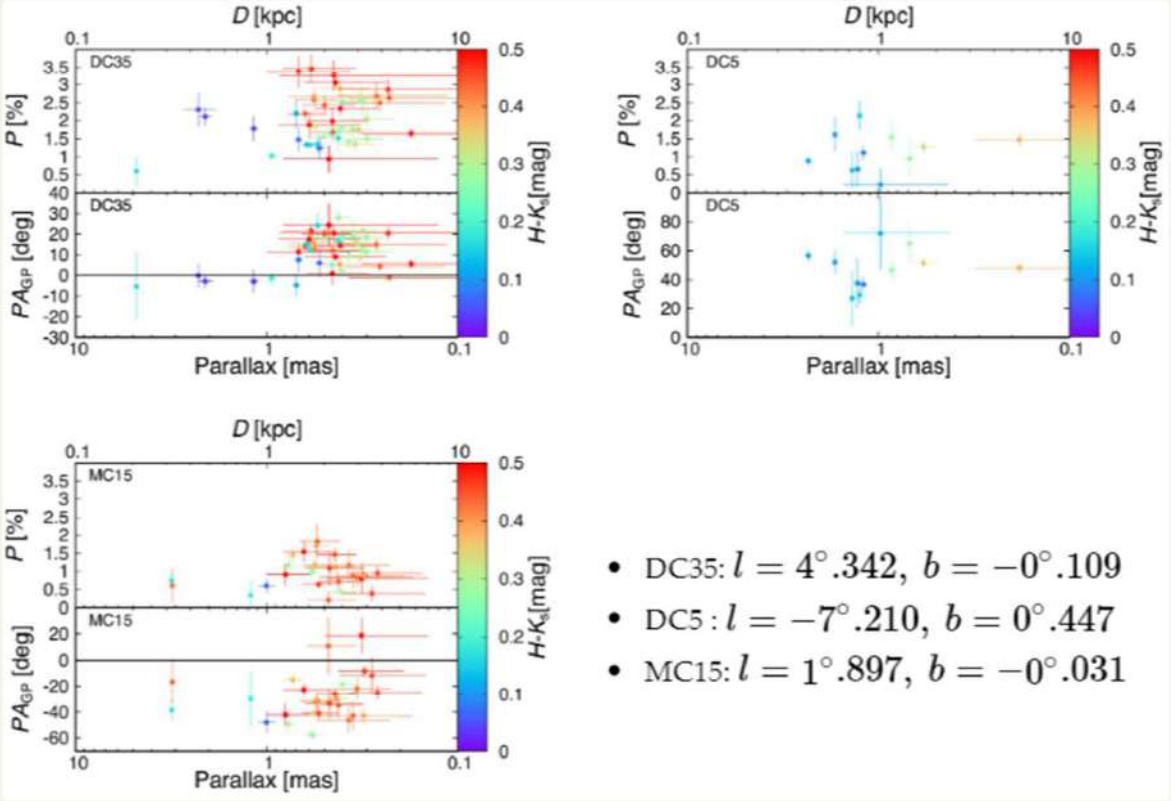

Zenko et al. (2020)

Besides local deviations, the new measurements of starlight polarization near the Galactic plane always confirm that the magnetic fields in the Galactic disk run parallel to the Galactic plane. – Han J. L., 2017, ARA&A, 55, 111.

Results: ditribution of *PA*

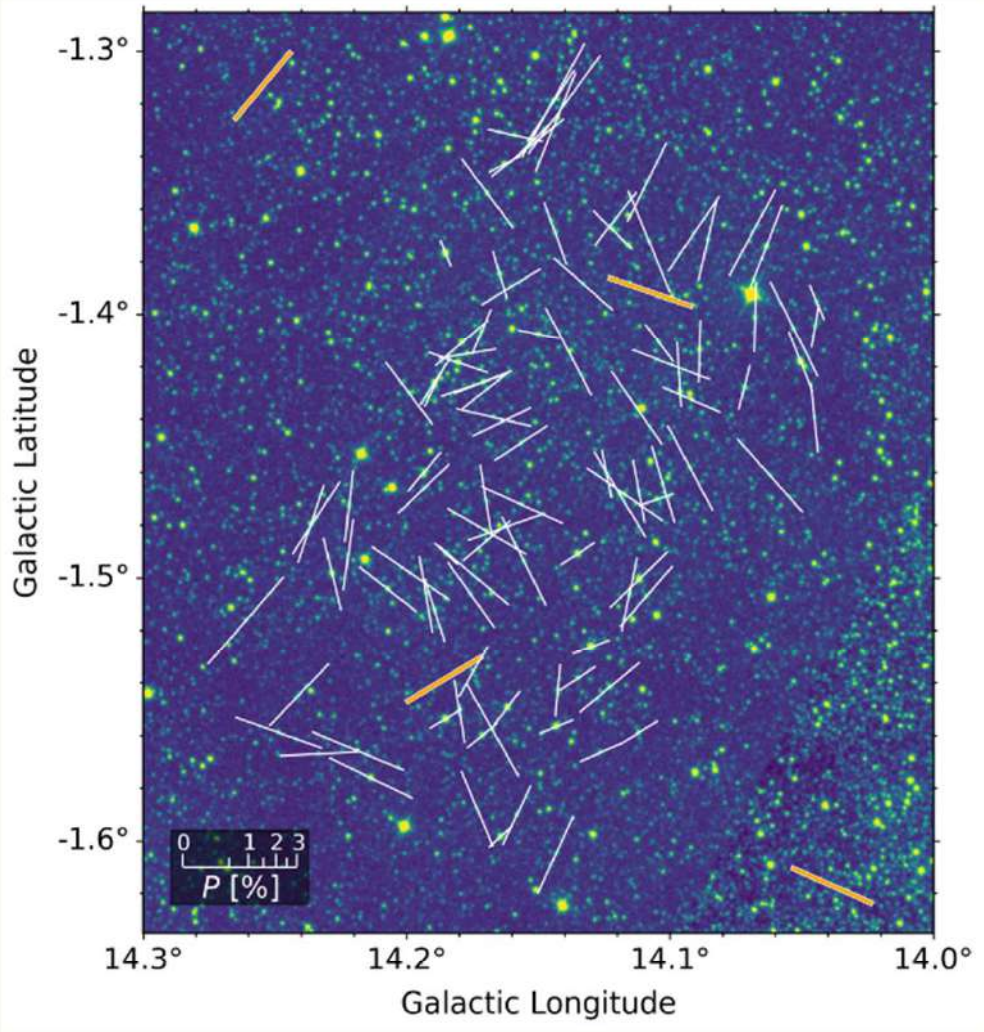

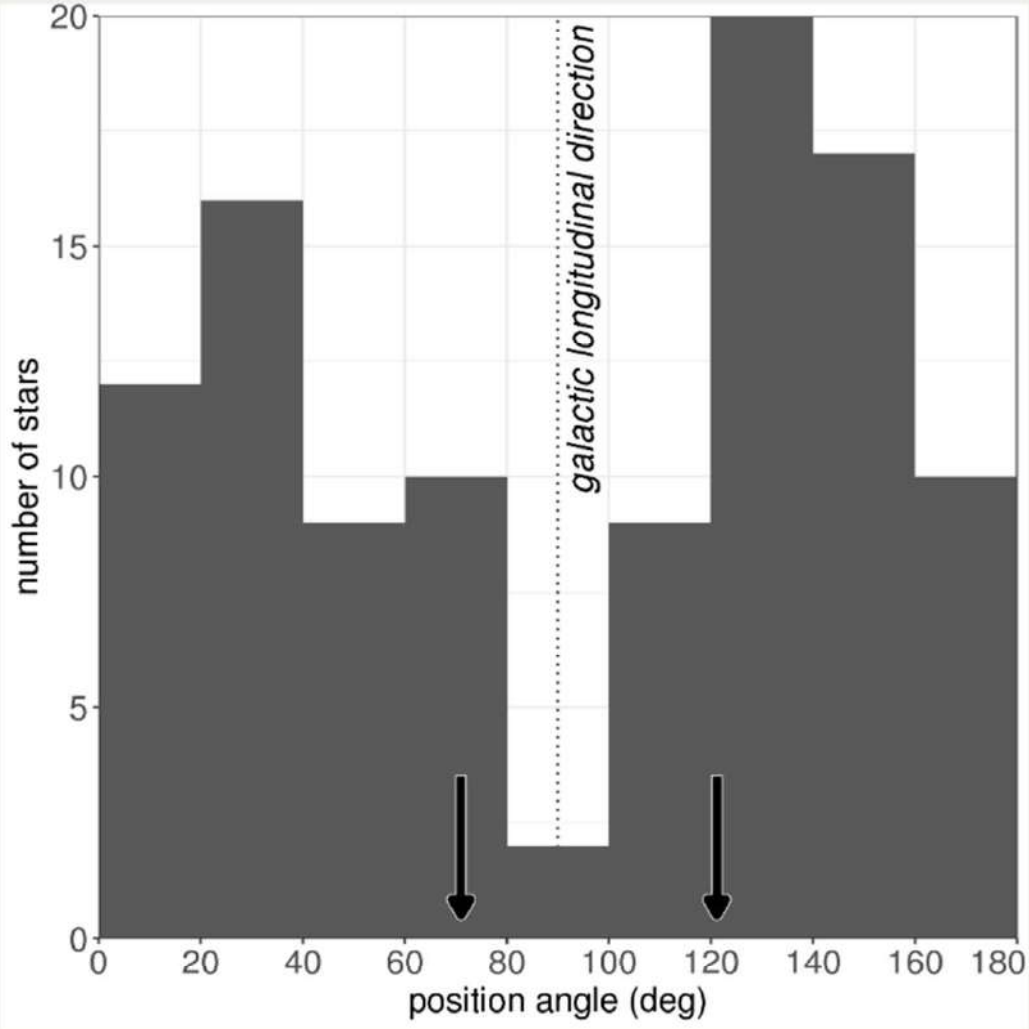

PA & *P* vs. stellar distance

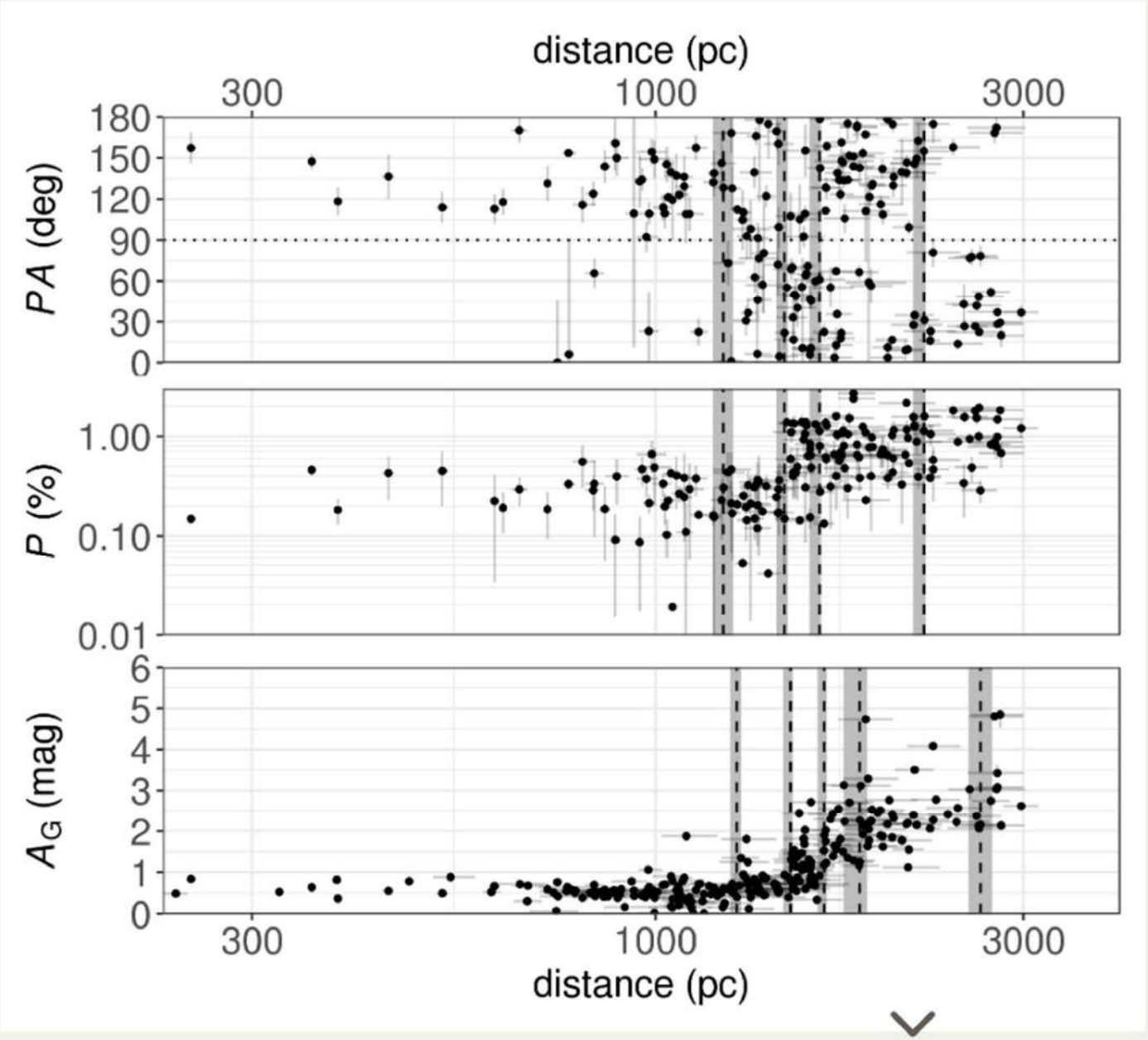

5 clouds with

$N_{\rm H} \simeq 1 \sim 3$

$\times 10^{21}\ ({\rm cm}^{-2})$

q & *u* cumulative plot

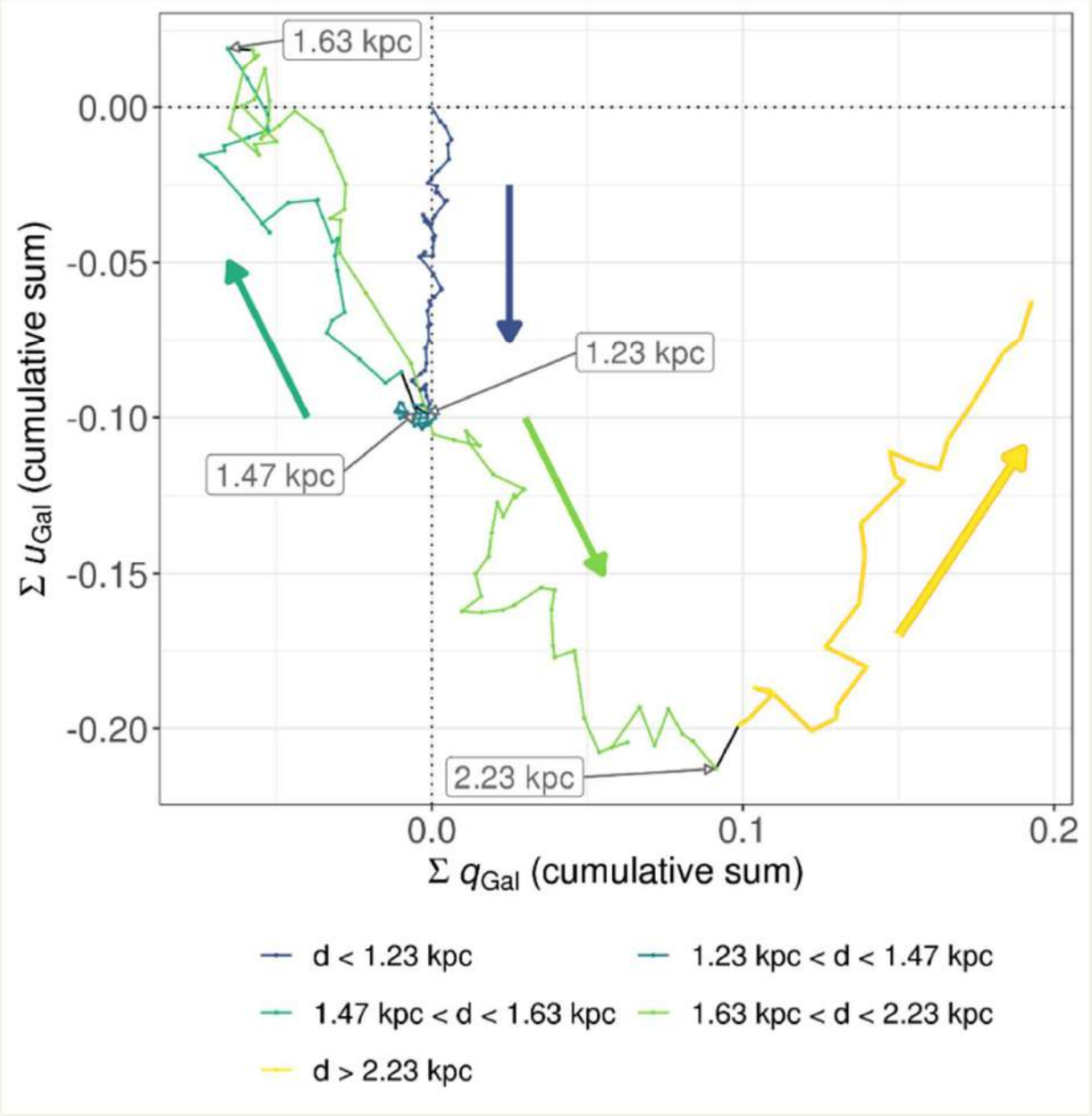

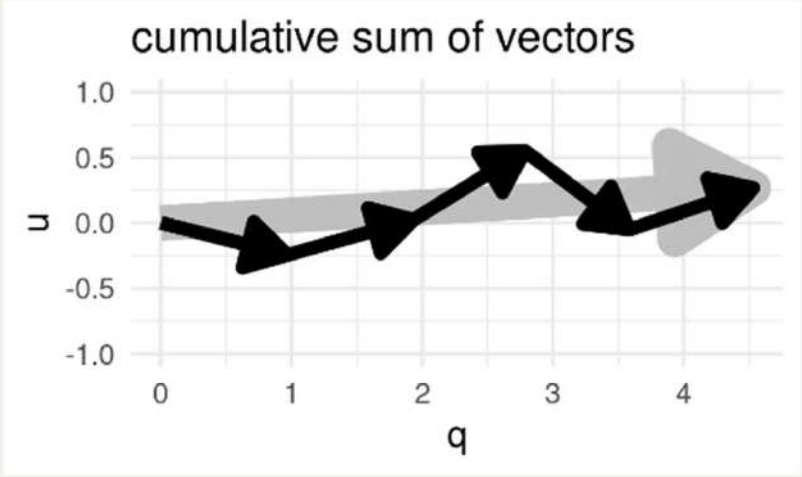

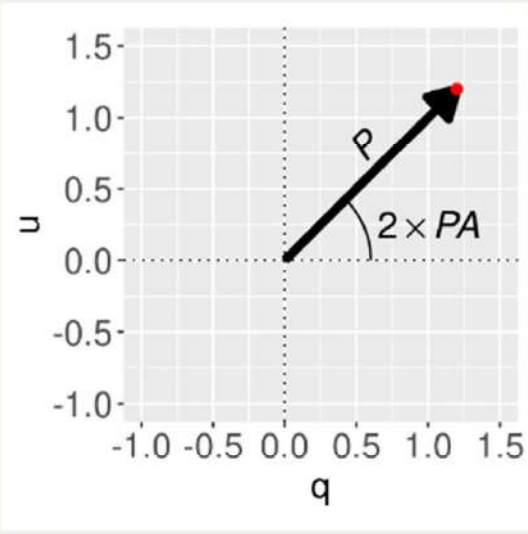

PA at each distance

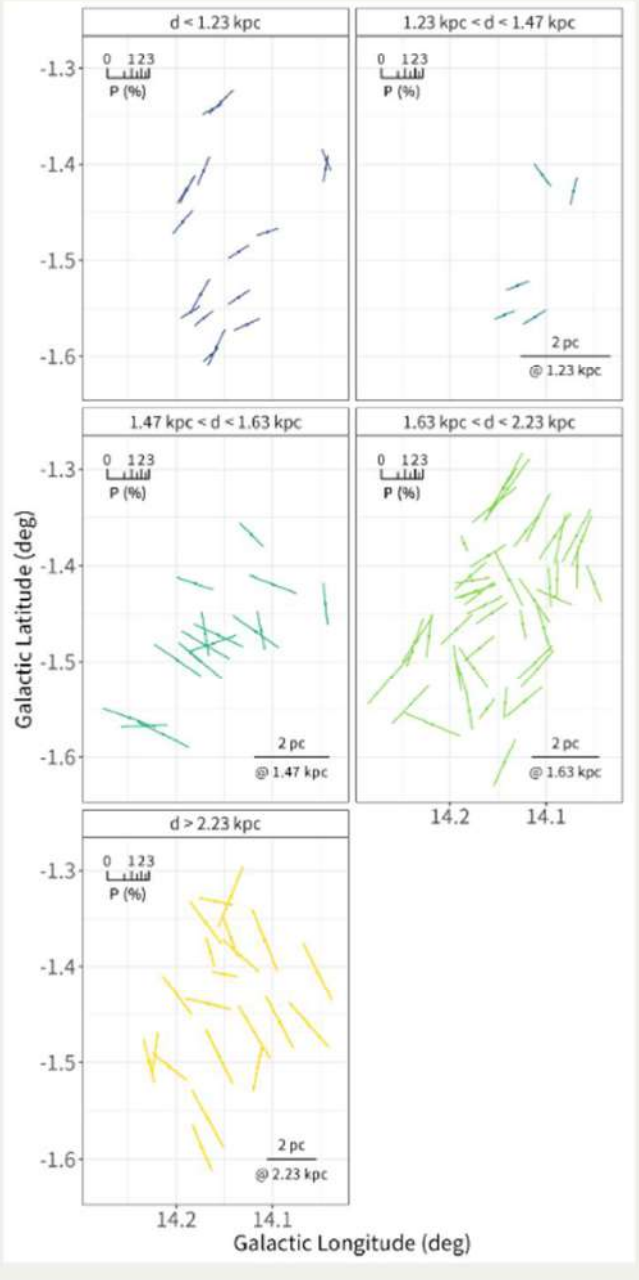

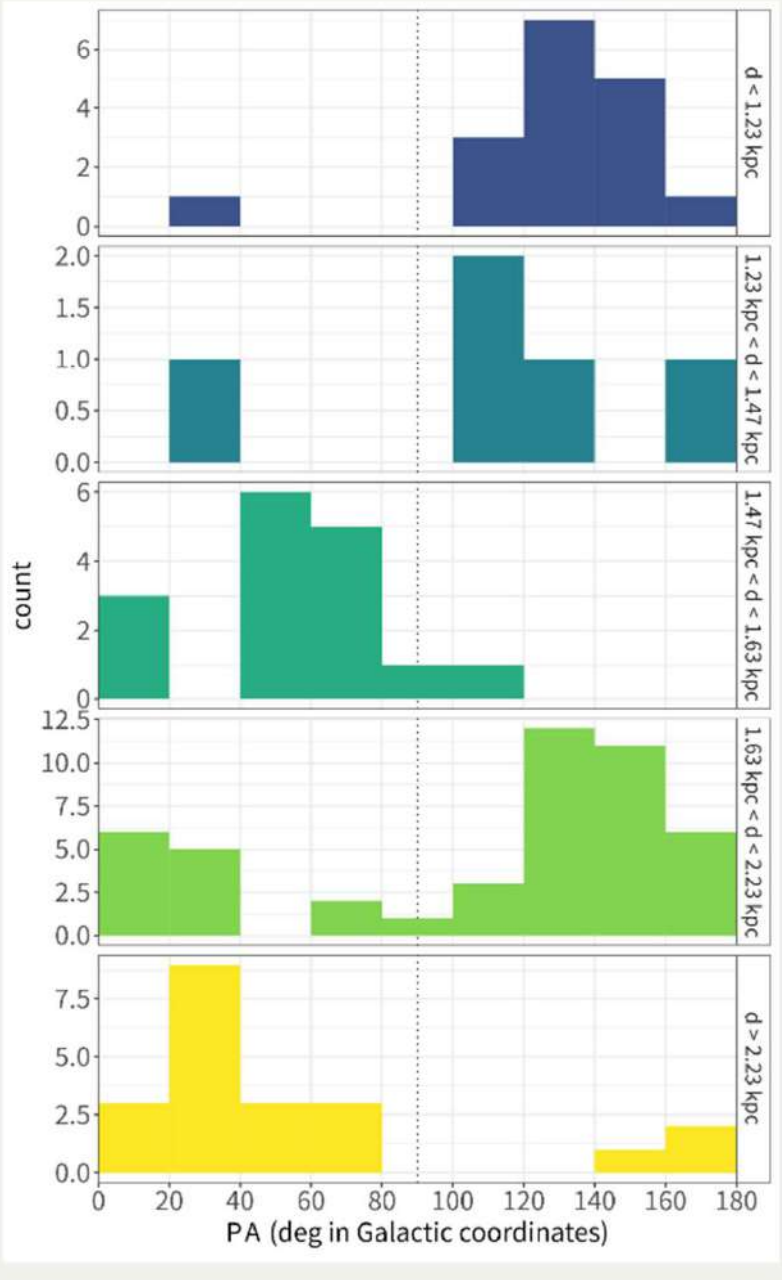

Polarization of individual clouds

- Take the difference on the q-u plane

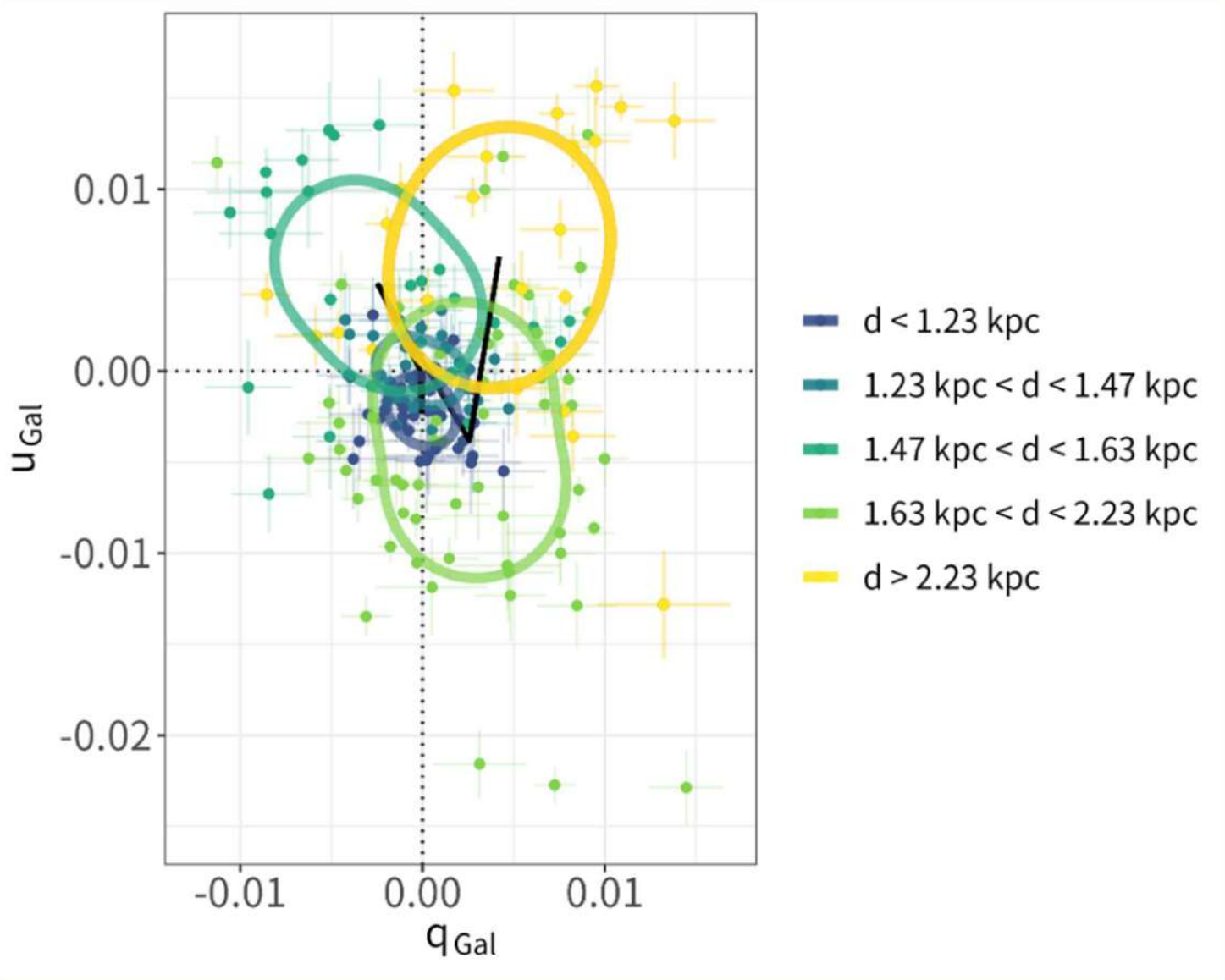

Polarization of individual clouds

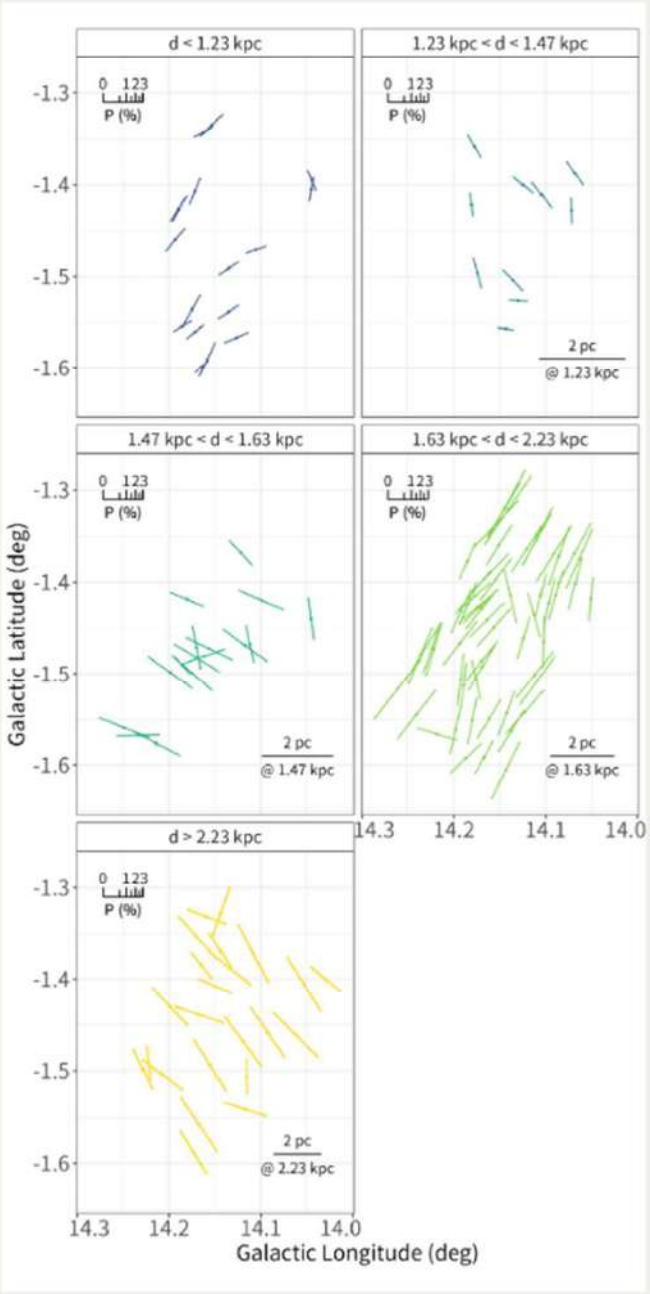

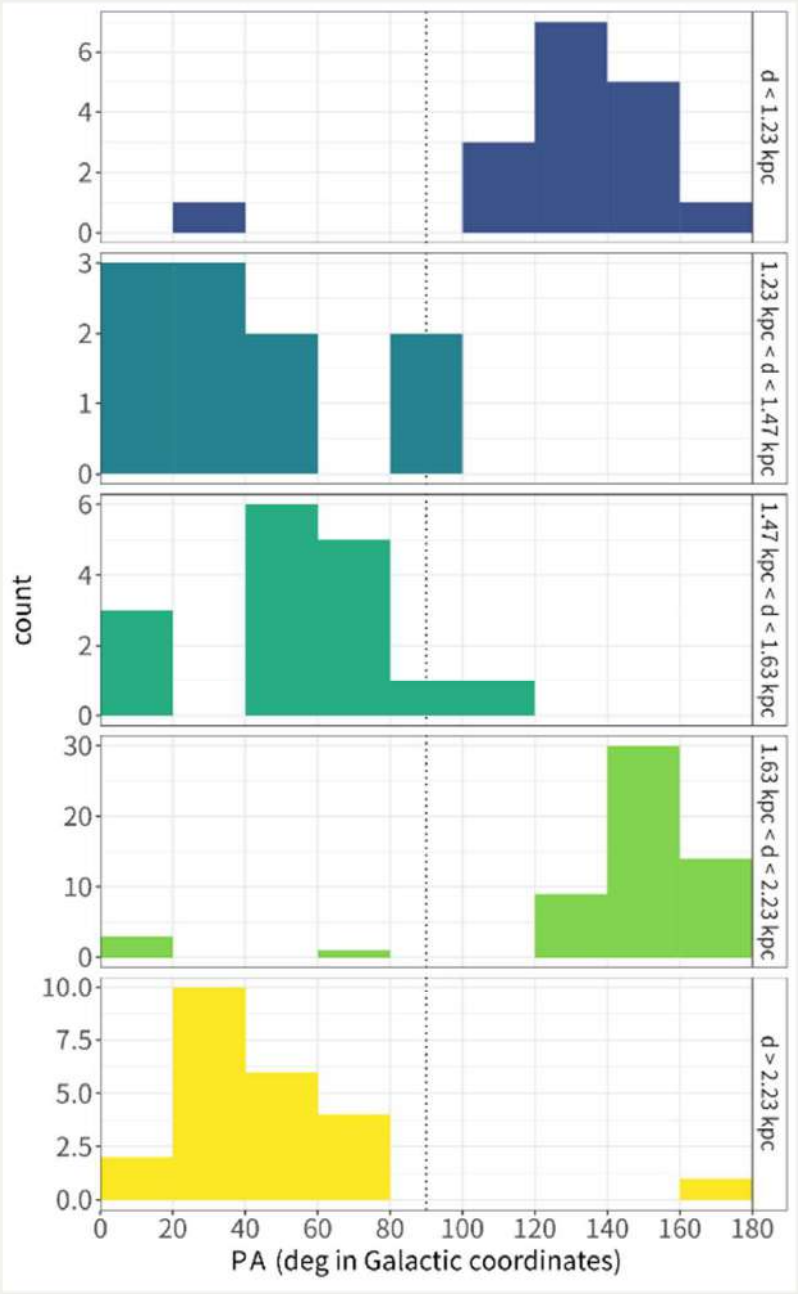

- Smooth distribution of the *B*-field at each distance range.
- Scale length: $\geqslant 10$ pc
- $N_{\rm H} \simeq 1 \sim 3 \times 10^{21}\ ({\rm cm}^{-2})$
- $\sigma^2_{PA} = \sum_i \sigma^2_{PA(i)}$ (not subtracted here)

Anti-correlation between σ_{PA} & p

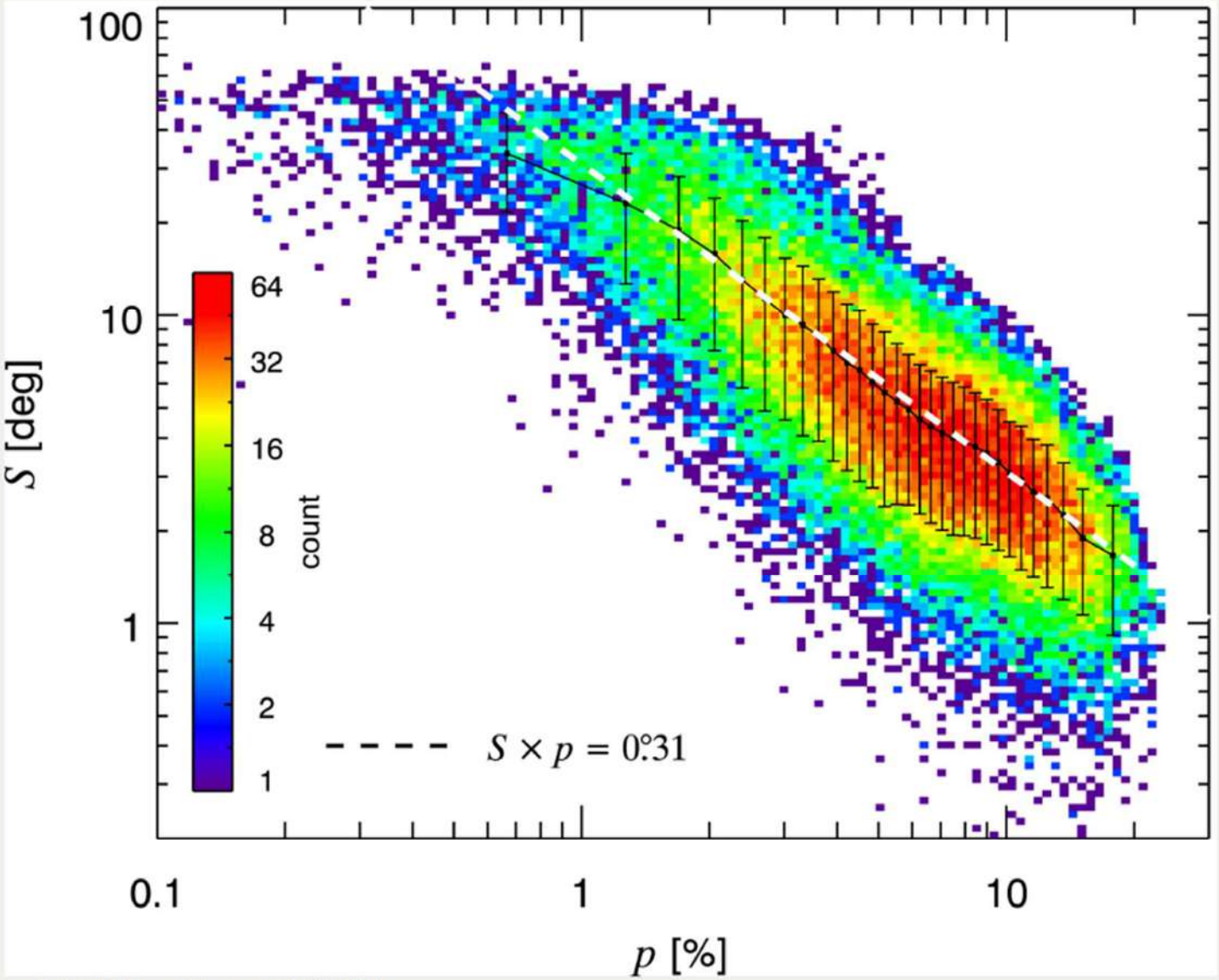

Planck Collaboration et al.(2020)

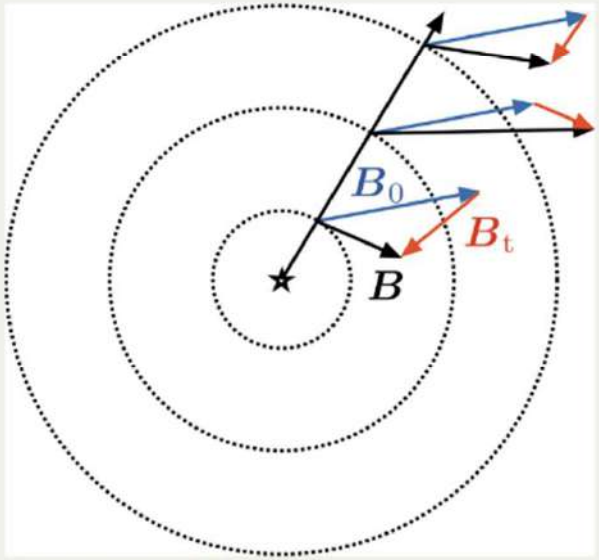

Their toy model.

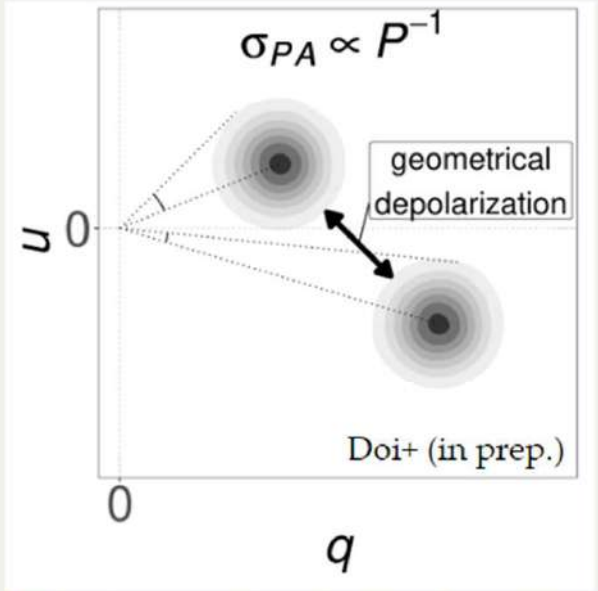

Shift on the q-u plane by depolarization

Anti-correlation due to the `shift' of the origin of the *q-u* plane

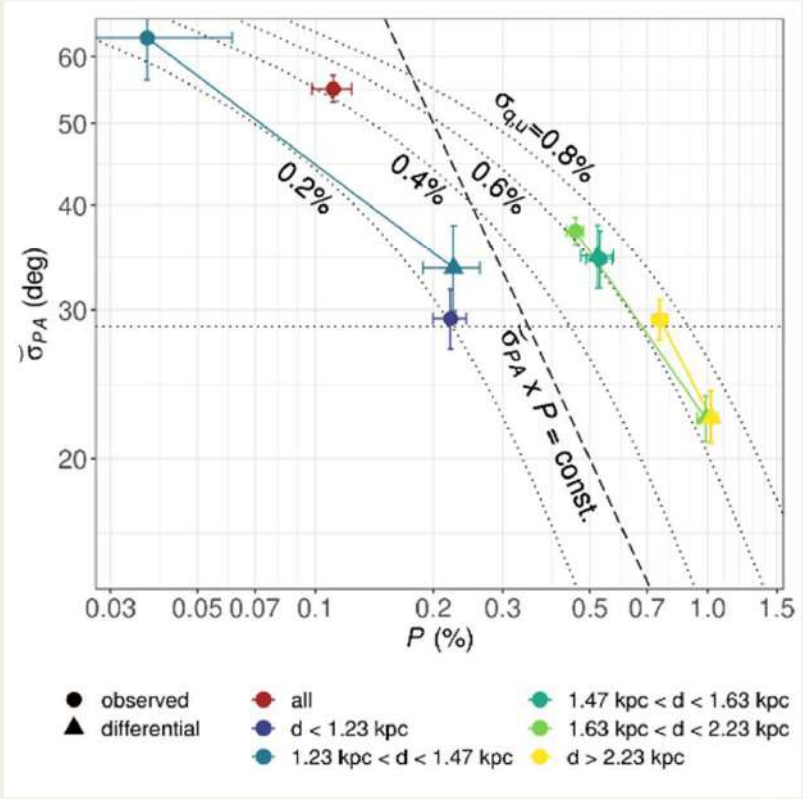

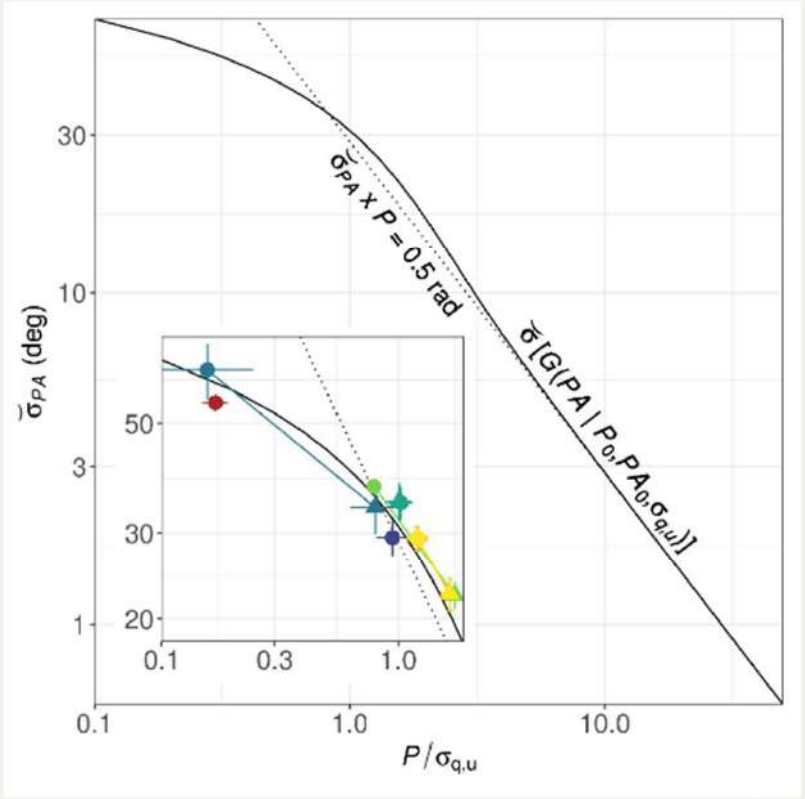

$$G(PA \mid p_0, PA_0, \sigma_{q,u}) = \frac{1}{\sqrt{\pi}}\left(\frac{1}{\sqrt{\pi}} + \eta_0 e^{\eta_0^2}\left[1 + \mathrm{erf}(\eta_0)\right]\right) e^{-\frac{p_0^2}{2\sigma_{q,u}^2}},$$

$$\eta_0 = \frac{P_0}{\sqrt{2}\sigma_{q,u}}\cos(2(PA - PA_0))$$

Geometrical depolarization makes the anti-correlation

- Optical and Planck polarimetries are on the same `anti-correlation' trend caused by the geometrical depolarization
- $\sigma_{PA} \propto (P/\sigma_{q,u})^{-1}$
- $\sigma_{q,u} \propto N_{\rm H} \times P/N_{\rm H} \times \sigma_{PA}$
  $=$ (column density) $\times$ (polarization efficiency) $\times$(turbulent magnetic field)

Characteristics of individual clouds

Cloud	PA (deg)	P (%)	$N_{\rm H}$ (10^{21} cm^{-2})	Pol.Efficiency (%/mag)	δPA (deg)	$\|B\|$ (μG)
foreground	$134.5^{+2.8}_{-2.8}$	$0.22^{+0.02}_{-0.02}$	$1.48^{+0.01}_{-0.01}$	$0.42^{+0.04}_{-0.04}$	$27.4^{+4.1}_{-5.0}$	$12.0^{+2.7}_{-1.5}$
1.23 kpc	$46.1^{+4.7}_{-4.8}$	$0.22^{+0.04}_{-0.04}$	$0.47^{+0.02}_{-0.02}$	$1.35^{+0.24}_{-0.23}$	$21.4^{+9.8}_{-21.4}$	$15.3^{+\infty}_{-4.7}$
1.47 kpc	$58.1^{+2.8}_{-2.8}$	$0.52^{+0.05}_{-0.05}$	$1.14^{+0.02}_{-0.02}$	$1.28^{+0.13}_{-0.12}$	$26.8^{+3.3}_{-3.8}$	$12.3^{+2.0}_{-1.4}$
1.63 kpc	$150.2^{+1.5}_{-1.4}$	$0.99^{+0.05}_{-0.05}$	$2.76^{+0.03}_{-0.03}$	$1.00^{+0.05}_{-0.05}$	$8.0^{+3.1}_{-4.3}$	$41.3^{+50.8}_{-11.4}$
2.23 kpc	$40.3^{+1.2}_{-1.2}$	$1.02^{+0.04}_{-0.04}$	$2.09^{+0.05}_{-0.06}$	$1.37^{+0.07}_{-0.06}$	$8.4^{+3.5}_{-4.0}$	$39.2^{+35.1}_{-11.5}$

- *cf.* Polarization efficiency $\simeq 1.5$ (%/mag) @ Perseus & Taurus (Doi+2021)
  - Efficiency differences $\leftrightarrow$ Inclined B-field to the plane of the sky?
- B-field strength: based on the DCF method, $|B| \propto \left(\frac{n_{\rm H}}{10^2\ {\rm cm^{-3}}}\right)^{1/2} \left(\frac{\Delta V_{\rm FWHM}}{5\ {\rm km\ s^{-1}}}\right)$

Magnetically sub-critical/super-critical transition ($N_{\rm H} \sim 10^{21}$ cm^{-2})

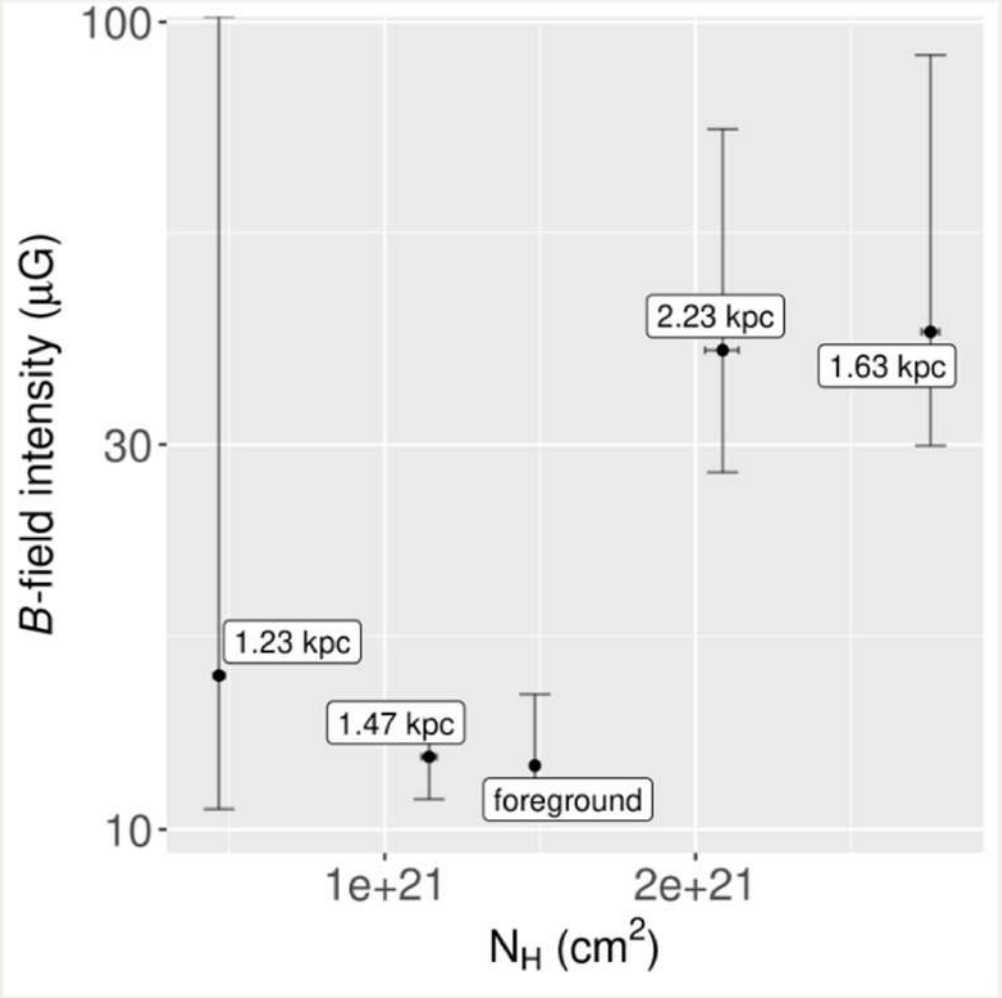

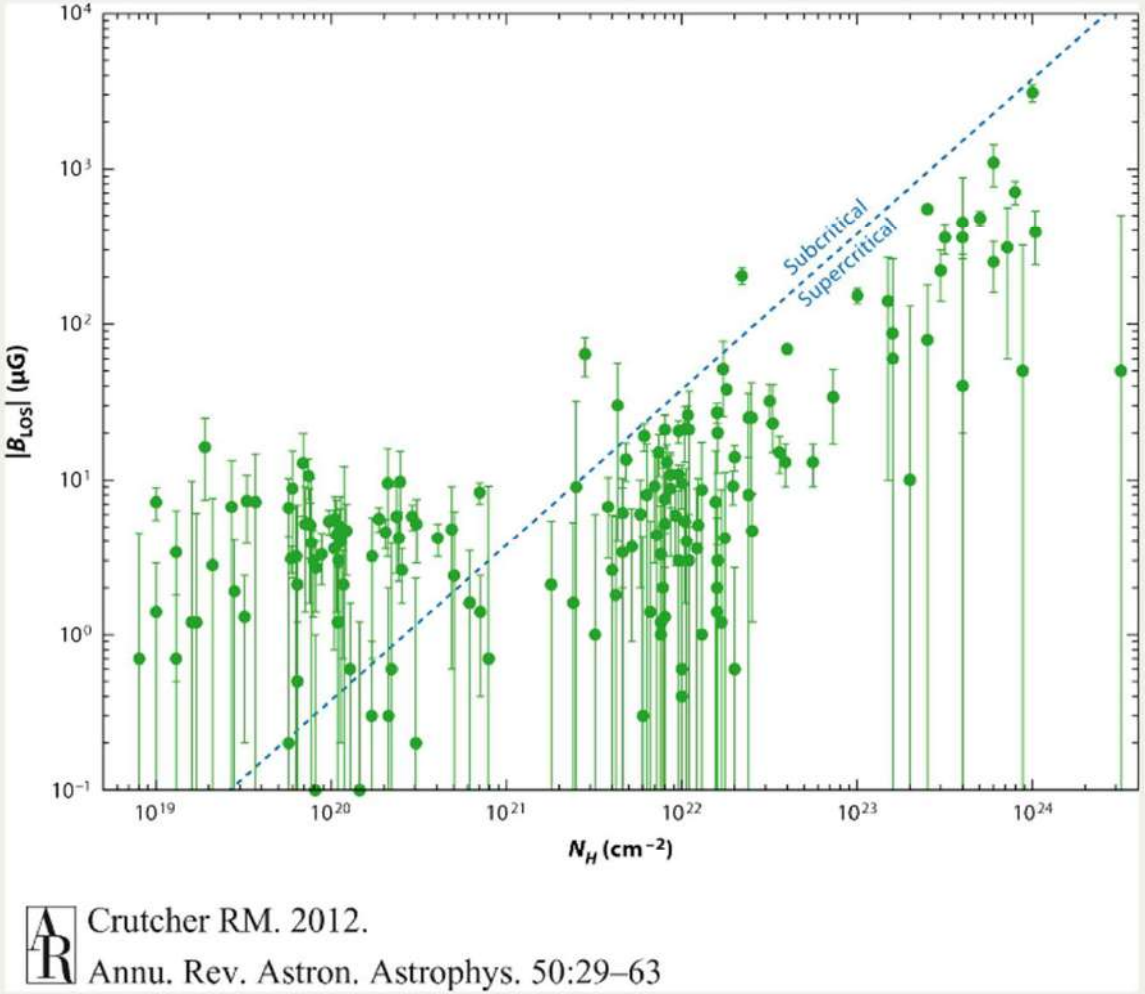

Crutcher RM. 2012.
Annu. Rev. Astron. Astrophys. 50:29–63

Additional Obs.

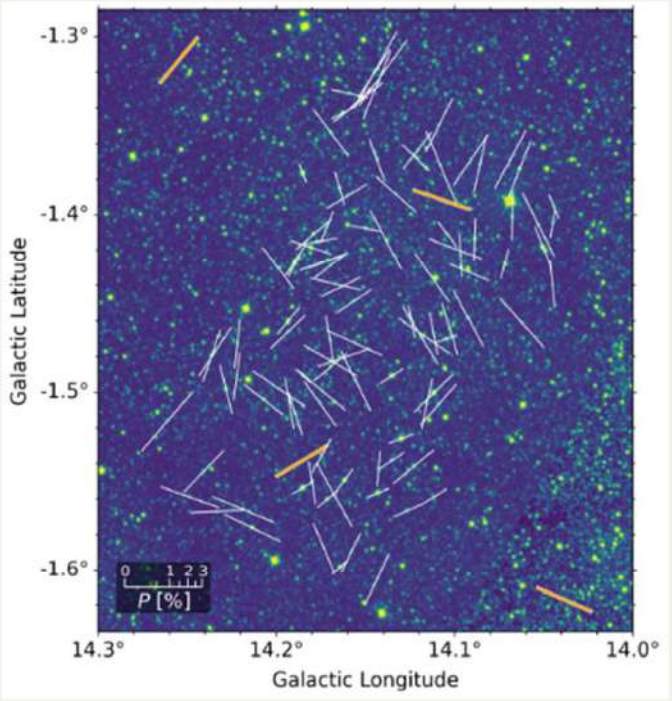

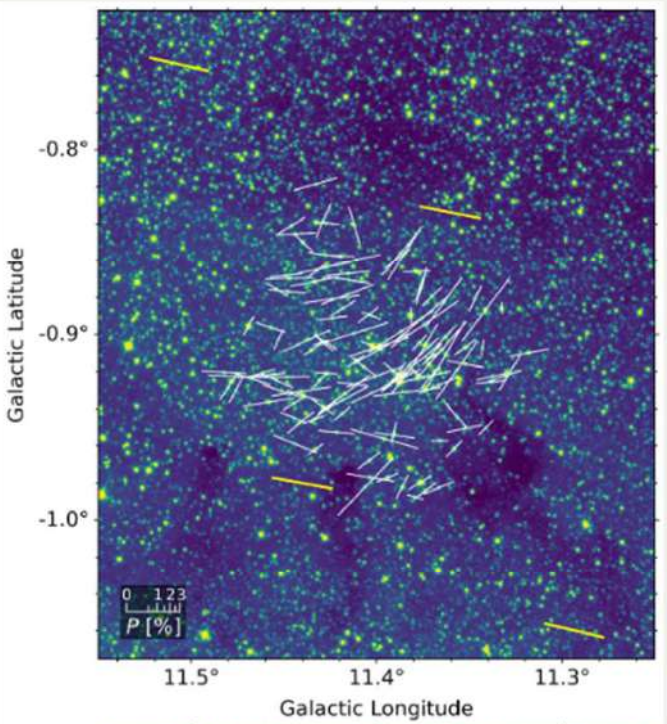

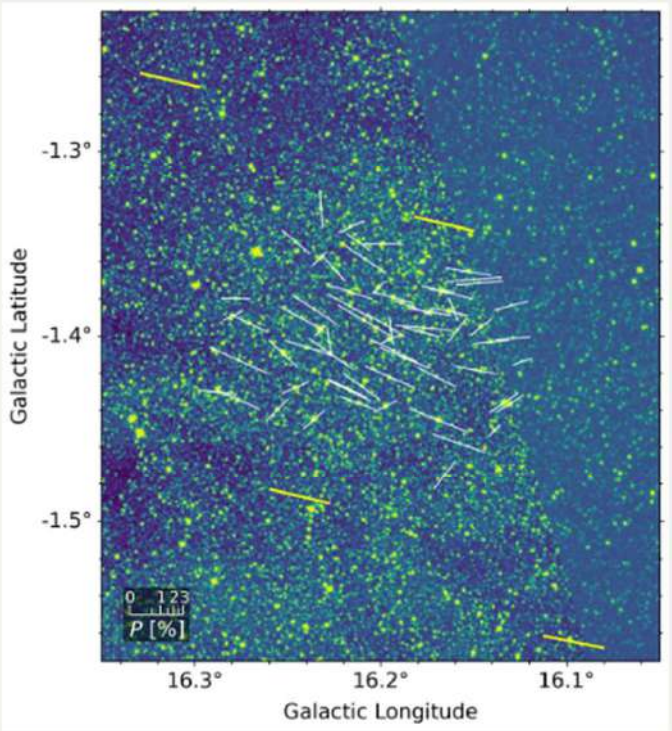

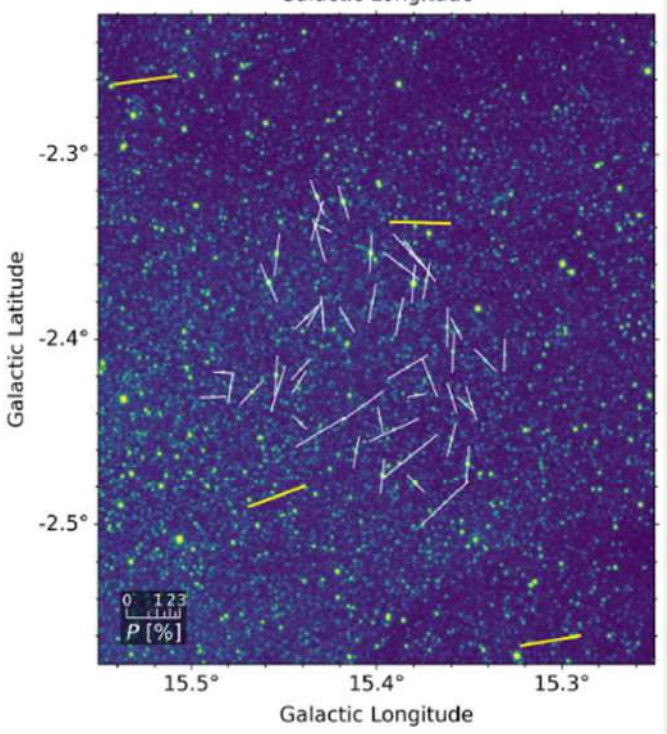

Large-scale *B*-field & ISM structures?

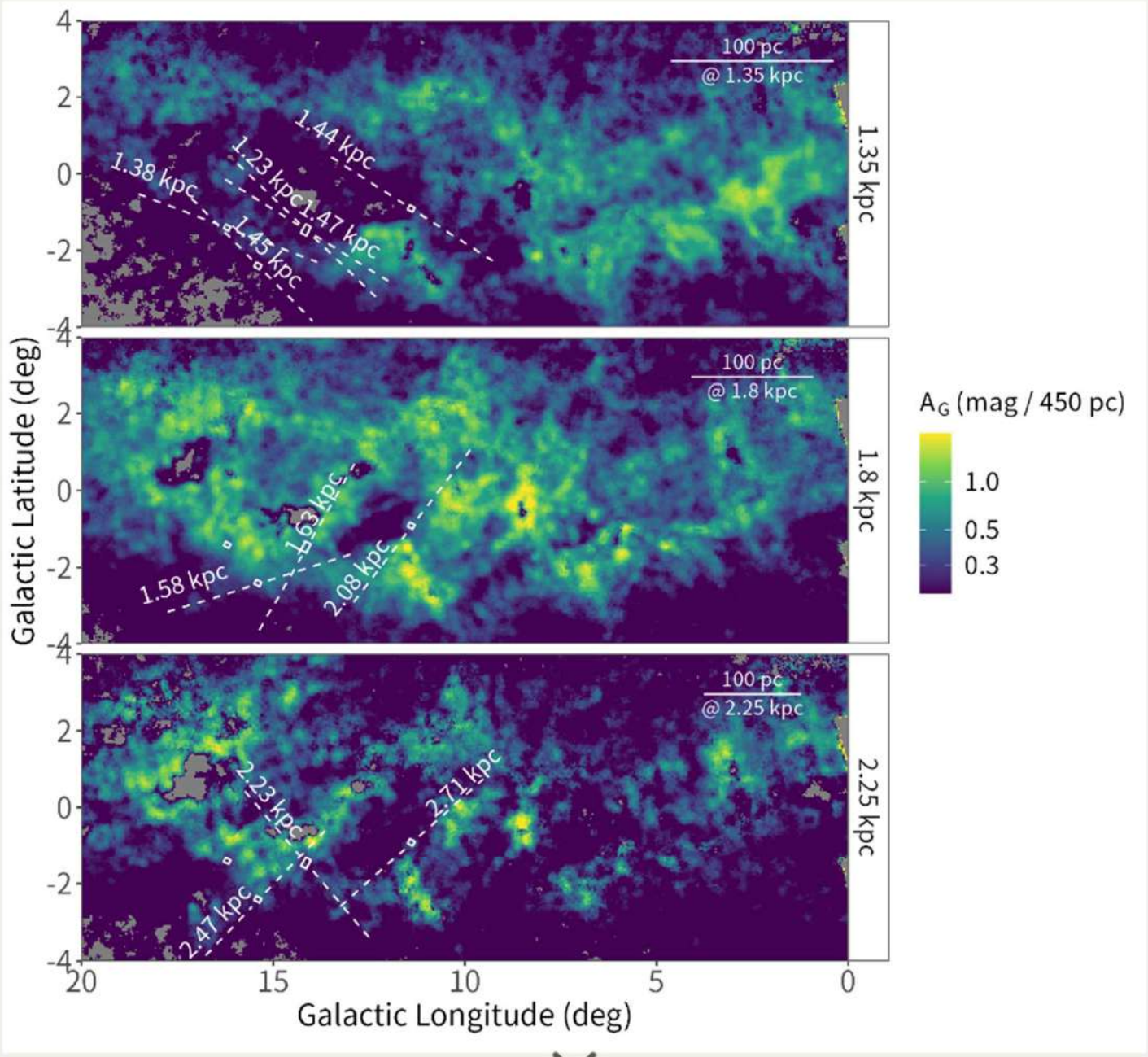

Summary

- Clear detection of multiple PA flips along the line-of-sight/inside a Galactic arm.
- No component parallel to the Galactic plane (in coordinates).
- Smooth distribution of the *B*-field ($\lesssim 10$ pc) associated with individual clouds.
- Large-scale *B*-field Alignment/Flipping over ~ 100 pc scale?

Near-future Plan

- Strategic field selection of characteristic regions in the Sagittarius arm
- Reveal the large-/small-scale 3D *B*-field in the arm